Numerical evidence of smooth self-similar dynamics and possibility of subsequent collapse for three-dimensional ideal flows

M. E. Brachet
Laboratoire de Physique Statistique, CNRS URA 1306, ENS Ulm, 24 rue Lhomond, 75231 Paris Cedex 05, France

M. Meneguzzi and A. Vincent
CERFACS, 42 Av. G. Coriolis, 31 000 Toulouse, France

H. Politano and P. L. Sulem
Observatoire de la Côte d'Azur, CNRS URA 1362, BP 229, 06304 Nice Cedex 4, France

(Received 29 April 1992; accepted 18 August 1992)

Direct numerical simulations of the three-dimensional Euler equations at resolutions up to 256^3 for general periodic flows and 864^3 for the symmetric Taylor–Green vortex are presented. The spontaneous emergence of flat pancakelike structures that shrink exponentially in time is observed. A simple self-similar model that fits these observations is discussed. Focusing instabilities similar to those leading to streamwise vortices in the context of free shear layers [J. Fluid Mech. **143**, 253 (1984)], are expected to subsequently concentrate the vorticity and produce isolated vortex filaments. A finite time singularity for the Euler equation is not excluded as the result of interactions among these filaments.

I. INTRODUCTION

A main characteristic of incompressible three-dimensional flows is vortex stretching. It is usually believed (but not yet proved mathematically) that in real fluids, this effect is interrupted by viscous diffusion after sufficiently small scales have been formed. In contrast, in an ideal fluid the question arises whether vorticity can be stretched an infinite amount in a finite time, leading to singularities for the Euler equation. A physical motivation for this study is the relation between these possible singularities and the small-scale-structures of boundary-free turbulence in the limit of infinite Reynolds numbers.

The only rigorous results for the Euler equation in three dimensions are local in time. For initial conditions corresponding to a vorticity which is differentiable (or at least Hölder continuous), a solution exists and preserves its initial regularity for a finite time. A simple proof is given in Ref. 1. In particular if the velocity is initially analytic, it remains so as long as the vorticity is Hölder continuous.[2] Results of local existence were also proved in Sobolev spaces for solutions with finite energy.[3] In this frame, occurrence of a singularity at a finite time t_* requires that the maximum vorticity blows up faster than $(t_*-t)^{-1}$. Conversely, if the strain tensor remains bounded, a smooth solution exists for all time. [4]

The existence of a finite time singularity for the Euler equation was conjectured on the basis of phenomenological turbulence models which do not retain the geometric structure of the high vorticity regions (see Ref. 5 for review). A singularity was also suggested by analyzing the variation of the energy dissipation in direct numerical simulations of the Navier–Stokes equations when the viscosity is decreased: a singularity is suspected if the amplitude and time of the maximum dissipation seem to converge to finite limits.[6,7] This analysis is in fact rather delicate since it involves simultaneous asymptotics on viscosity and time. An indication of singularity was also obtained in Ref. 8 for the so-called Taylor–Green vortex,[9] using analytic continuation techniques on temporal Taylor series of the solutions beyond the convergence disk by means of Padé approximants. This result was questioned in Ref. 10 where it was pointed out that accuracy in the analytic continuation deteriorates too quickly to lead to any definite conclusion.

A more straightforward approach consists in the direct simulation of the inviscid problem during a time consistent with the spatial resolution. An indication of global regularity was obtained by monitoring the vorticity maximum, for an initial condition consisting in two vortex tubes.[11] The algorithm was a finite-difference scheme with an adaptive mesh. Evidence of a singular behavior was, however, reported by these authors in the case of axisymmetric flows.[12] Still considering the time evolution of vorticity but using spectral methods, presumptions of finite time singularity were presented in Ref. 13.

Finite-difference schemes with adaptive mesh enable one to integrate during relatively long times. Nevertheless, it is rather difficult to control the accuracy in the resolution of the smallest scales and the computation of the vorticity maximum.

In the case of space-periodic flows, a more robust approach is provided by the analyticity strip method[14] based on the tracing of complex space singularities as time evolves. Assume that at a given time, the solution can be continued to complex space variables $\mathbf{x}+i\mathbf{y}$ inside the analyticity strip $|\mathbf{y}|<\delta$. The width δ can easily be derived from the large-wave-number behavior of the spatial Fourier transform of the solution. Indeed, for large k, the amplitude of the Fourier modes decreases like $e^{-\delta k}$ (up to an algebraic prefactor). For an initial value problem, it is possible to measure δ accurately as long as it remains larger than a few mesh sizes. During this whole time interval, spectral convergence of the Fourier expansion is ensured, a

 0899-8213/92/122845-10$04.00

condition requested to resolve precisely the smallest scales of the exact solution.

The analyticity strip method is especially adapted to the Euler equation since, as already mentioned, for analytic initial data, low-order derivatives of the velocity field blow up when analyticity is lost. It was used in Ref. 10 for the inviscid Taylor–Green vortex. Resolutions up to 256^3 collocation points were reached on a Cray-1, by implementing the specific properties of this highly symmetric flow in the numerical algorithm. It appeared that, as long as the computation was reliable, δ was decreasing exponentially in time. If this behavior can be extrapolated indefinitely, it would correspond to global existence of analytic solutions for the three-dimensional Euler equation.

The aim of the present paper is to examine thoroughly the regularity properties of the three-dimensional Euler equation, based on numerical simulations at the highest available resolutions on a 256 Mwords, 4 processors Cray-2. In Sec. II, the numerical algorithms are briefly presented for initial conditions corresponding to both the Taylor–Green vortex and random periodic data with an initial energy spectrum peaked at small wave numbers. In Sec. III, the analyticity properties of the flow are derived from the large-wave-number behavior of the energy spectrum, using the analyticity strip method. In Sec. IV, visualizations in physical space of high vorticity regions, in the form of "vorticity pancakes" are displayed. A simple model of self-similar evolution which fits the numerical observations is also presented. In Sec. V, a possible mechanism for a subsequent instability of the vorticity pancakes focusing into vortex tubes is discussed. Sec. VI is the conclusion.

II. THE NUMERICAL APPROACH

The Euler equation

$$\partial_t \mathbf{v} + (\mathbf{v}\cdot\nabla)\mathbf{v} = -\nabla p, \qquad \nabla\cdot\mathbf{v} = 0, \tag{1}$$

is integrated numerically in a 2π-periodic box, using spectral methods. Time marching is done with a second-order leapfrog or Adams–Bashforth finite-difference scheme.

In a first series of runs, we considered the Taylor–Green vortex[9] which is an incompressible three-dimensional flow developing from the single mode initial conditions

$$v_x = \sin x \cos y \cos z, \qquad v_y = -\cos x \sin y \cos z, \qquad v_z = 0. \tag{2}$$

This flow displays several symmetries that are implemented in the numerical simulation in order to reduce memory requirement and operation number. With the same code as the one used to simulate viscous flows,[15] inviscid calculations at resolutions up to 864^3 collocation points were performed. In this algorithm, the solution is dealiased by suppressing at each time step the Fourier modes for which at least one wave-vector component exceeds two-thirds of the wave-number cutoff.

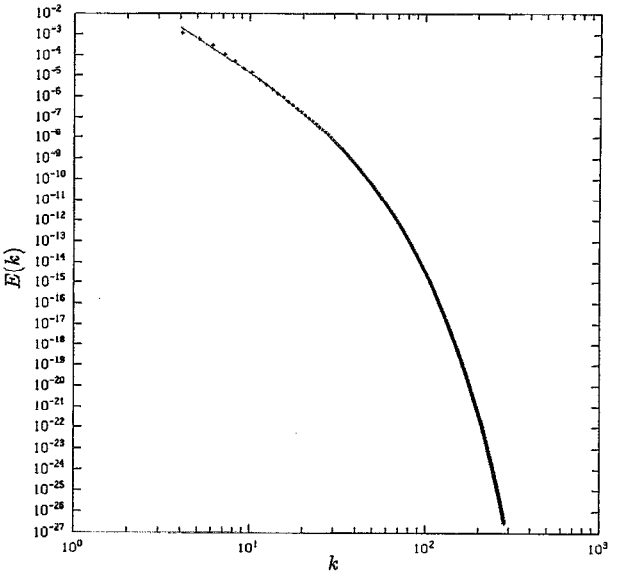

FIG. 1. Energy spectrum $E(k)$ (crosses) together with a mean-square fit (solid line) of the form $ck^{-n}e^{-2\delta k}$ for the Taylor–Green vortex with a resolution of 864^3, at time $t=2.1$. The fit is performed in the range $5<k<279$.

We also considered random initial conditions with a spectrum of the form $E(k)=ck^2e^{-(k/k_0)^2}$ with $k_0=1$ and $c=0.03$. With the same code as the one described in Ref. 16, dealiased simulations at resolutions up to 256^3 were performed. In order not to reduce significantly the effective resolution, aliasing was suppressed as in Ref. 17, a method which retains 94% of the maximum wave number but doubles the operation number.

At the maximum resolutions, our codes require all the machine memory. They are multitasked on the four CPU's in order to maximize the computing power.

III. SPECTRAL PROPERTIES

In the framework of spectral methods for problems with periodic boundary conditions, it is easy to investigate the regularity properties of the solution by implementing the analyticity strip method. It consists in analyzing the time evolution of the energy spectrum

$$E(k,t)=\frac{1}{2}\sum_{k-(\Delta k/2)<|\mathbf{k}'|<k+(\Delta k/2)} |\hat{\mathbf{v}}(\mathbf{k}',t)|^2, \tag{3}$$

obtained by averaging on spherical shells of width $\Delta k=1$. In Eq. (3), $\hat{\mathbf{v}}(\mathbf{k}',t)$ denotes the spatial Fourier transform of the solution.

As long as the velocity field is analytic, the energy spectrum $E(k,t)$ decays exponentially at large k (with a possible algebraic prefactor). The logarithmic decrement is twice the width $\delta(t)$ of the analyticity strip of the solution when continued to complex spatial variables. The temporal evolution of the analyticity strip is obtained by fitting the computed energy spectrum $E(k,t)$ with the assumed functional form

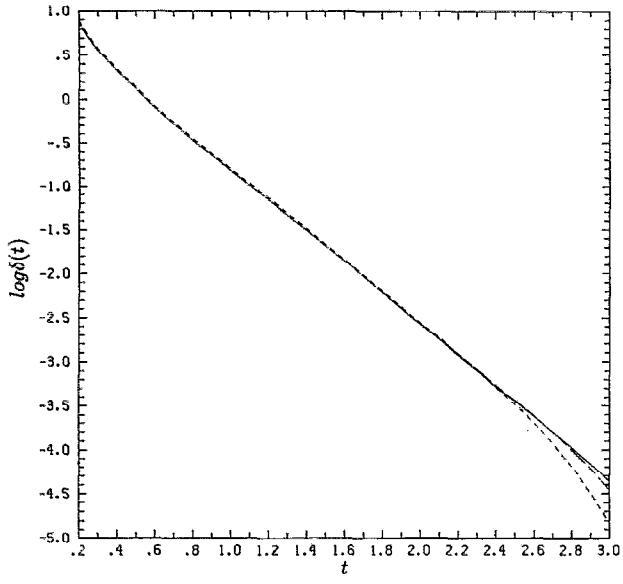

FIG. 2. Time evolution of the logarithmic decrement $\delta(t)$ obtained by fitting the energy spectrum on the ranges $5<k<71$, $5<k<161$, and $5<k<279$ for the inviscid Taylor–Green vortex integrated with resolutions 256^3 (dotted line), 512^3 (dashed line), and 864^3 (solid line), respectively.

$$c(t)k^{-n(t)}e^{-2\delta(t)k}. \tag{4}$$

An example of a mean-square fit of this form is presented in Fig. 1 for the Taylor–Green vortex at time $t=2.1$ when integrated at a resolution of 864^3 collocation points. The crosses give the computed energy spectrum while the solid line is the result of the fit performed in the range $5<k<279$. In order to avoid spectral oscillations resulting from the symmetries of the Taylor–Green flow, the energy spectrum was in this case averaged on shells of width $\Delta k=2$. Except at the lowest wave numbers where no universal behavior is expected, the fit appears to be very good.

The measure of $\delta(t)$ is reliable as long as it remains larger than a few mesh sizes, a condition required for the smallest scales to be accurately resolved and spectral convergence ensured. Figure 2 shows $\delta(t)$ versus time for the inviscid Taylor–Green vortex integrated at resolutions 256^3, 512^3, and 864^3. The fits of the energy spectrum were performed on ranges $5<k<71$, $5<k<161$, and $5<k<279$, respectively. We clearly see that after a short transient, $\delta(t)$ decays like

$$\delta(t)=\delta_0 e^{-t/T}, \tag{5}$$

with a characteristic shrinking time $T=0.57$ and $\delta_0=2.5$, up to a time $t=3$ when it becomes comparable to twice the smallest resolved scale.

Figures 3(a) and 3(b) display the time variation of the enstrophy

$$\Omega(t)=\int_0^{+\infty} k^2 E(k,t)\,dk \tag{6}$$

and of its normalized derivative

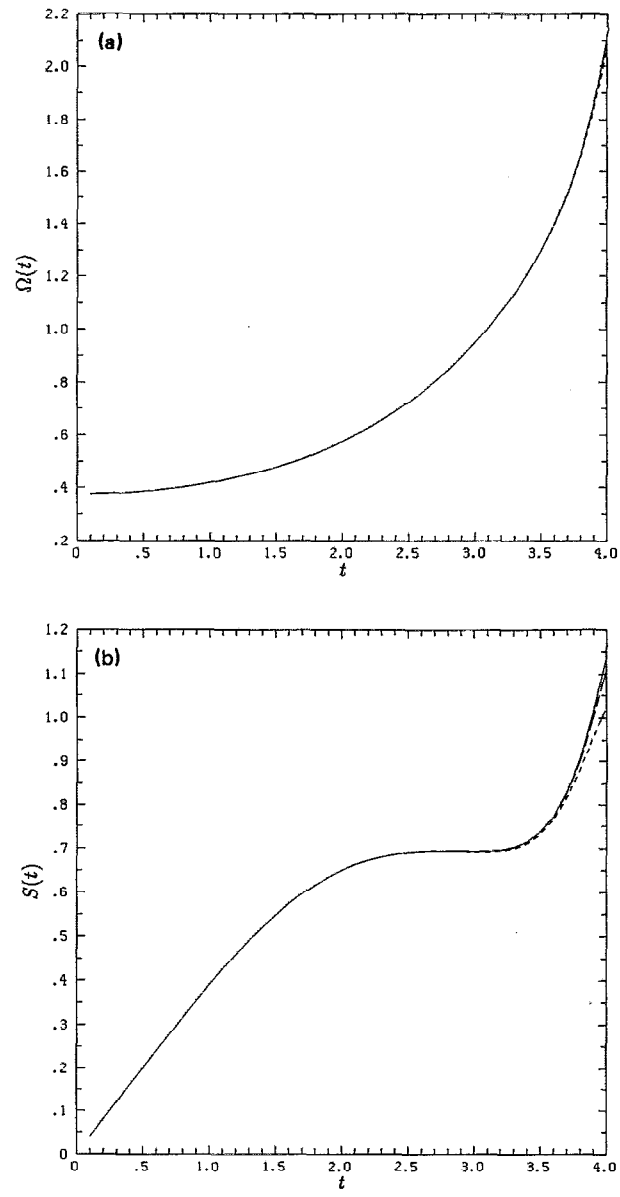

FIG. 3. Time variation of the enstrophy $\Omega(t)=\int_0^{+\infty} k^2E(k)\,dk$ (a) and of its normalized derivative $S(t)=(\frac{135}{98})^{1/2}[\dot{\Omega}(t)/\Omega(t)^{3/2}]$ (b), for the Taylor–Green vortex, at resolutions 256^3 (dotted line), 512^3 (dashed line), and 864^3 (solid line).

$$S(t)=\left(\frac{135}{98}\right)^{1/2}\frac{\dot{\Omega}(t)}{\Omega(t)^{3/2}} \tag{7}$$

(which identifies with the skewness when isotropy is assumed[6]), for the Taylor–Green vortex at resolutions 256^3, 512^3, and 864^3. We notice that the enstrophy remains insensitive to the resolution during a time significantly longer than the period during which the logarithmic decrement is accurately computed. An analogous phenomenon is visible on S at least for the two runs with the highest resolutions. The logarithmic decrement is indeed mostly sensitive to the small scales.

Assuming that the exponential decay of the logarithmic decrement of the Taylor–Green vortex can be extrapolated indefinitely, this would indicate that this flow re-

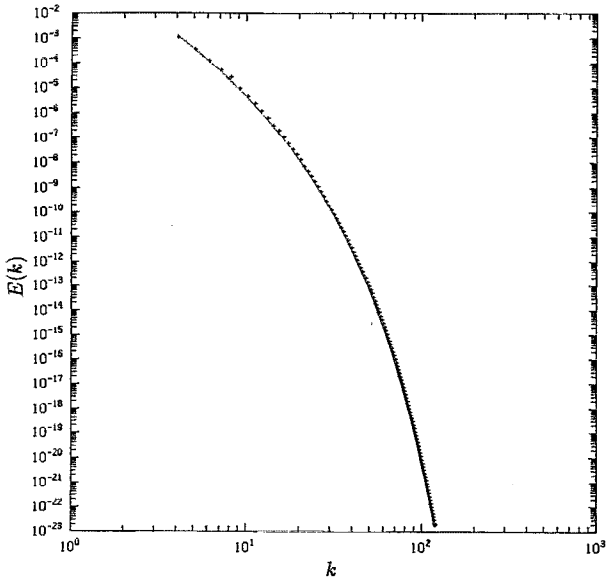

FIG. 4. Energy spectrum $E(k)$ (crosses) together with a mean-square fit (solid line) of the form $ck^{-n}e^{-2\delta k}$ for the random periodic flow with a resolution of 256^3, at time $t=1.2$. The fit is performed in the range $5<k<119$.

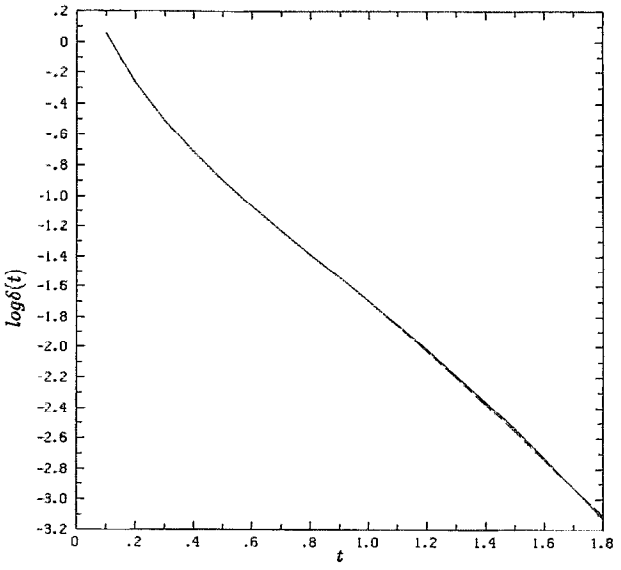

FIG. 5. Time evolution of the logarithmic decrement $\delta(t)$ for the general periodic flow, obtained by fitting the energy spectrum in the ranges $5<k<90$ and $5<k<110$, for simulations at resolutions 200^3 (dashed line) and 256^3 (solid line), respectively.

mains analytic for all times. On the other hand, it immediately follows from its definition that S should tend to zero when t goes to infinity in order to prevent a finite-time blowup of the enstrophy. Such a decay is not visible on Fig. 3(b) where S is seen to grow monotonically. The integration time is in fact too short to reveal the asymptotic behavior of S and Ω.

We now turn to simulations of general periodic flows with random initial conditions in order to check the genericness of the results obtained with the Taylor–Green vortex. The latter indeed displays specific features, like symmetries and lines of zero vorticity. The initial conditions we chose correspond to an energy spectrum of the form $E_0(k)=ck^2\,e^{-(k/k_0)^2}$ with $k_0=1$ and $c=0.03$. In the case of the realization we used, the initial energy $E_0=6.5\times10^{-2}$ and the initial enstrophy $\Omega_0=0.29$. Dealiased numerical simulations were performed at resolution 200^3 and 256^3 collocation points. Figure 4 shows that the energy spectrum is again well fitted with the functional form (4). An essentially exponential decay is obtained for $\delta(t)$, up to the moment when it becomes of the order of a few mesh sizes and the accuracy of the simulation deteriorates (Fig. 5). This result strongly supports the genericity of the behavior observed for the Taylor–Green vortex.

In order to compare the approach mainly used in this paper, consisting of monitoring the logarithmic decrement of the energy spectrum, and the method consisting of following the time evolution of the vorticity maximum $\sup|\omega|$, the latter quantity is plotted in Fig. 6 in lin–log coordinates for the random periodic flow. We observe that the growth is exponential from $t\simeq0.1$ to 1.05, and also, but with a larger rate, from $t\simeq1.05$ to 2. Later on, spectral accuracy is lost. We observe that at the instant where the growth rate varies ($t\simeq1.05$ and 2), the position of the vorticity maximum displays a discontinuity, indicating a jump from one vorticity structure to another. This effect is also visible, although to a much less extent, on the logarithmic decrement (Fig. 5).

In addition to the logarithmic decrement, the representation of the energy spectrum by the functional form (4) provides the exponent $n(t)$. For both the Taylor–Green vortex and the random flow, we observed in Figs. 7(a) and 7(b) that $n(t)$ varies between 4 and 5, and appears to approach 4 at the end of the runs. A similar observation is

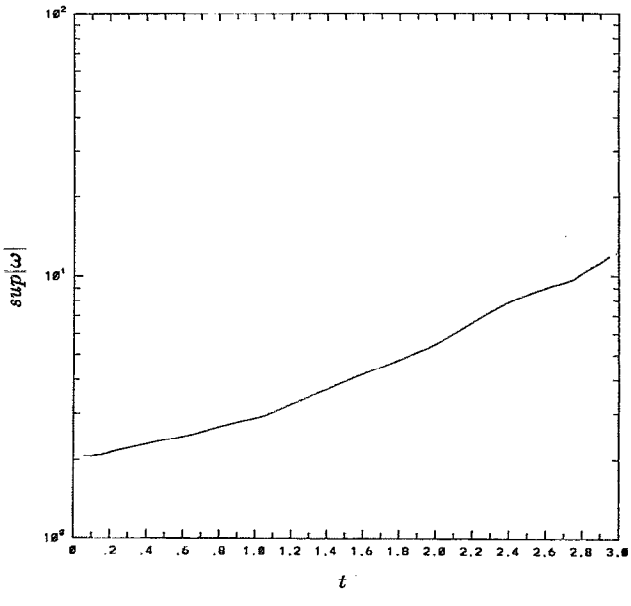

FIG. 6. Time evolution of the vorticity maximum $\sup|\omega|$ for the random periodic flow at resolution 256^3.

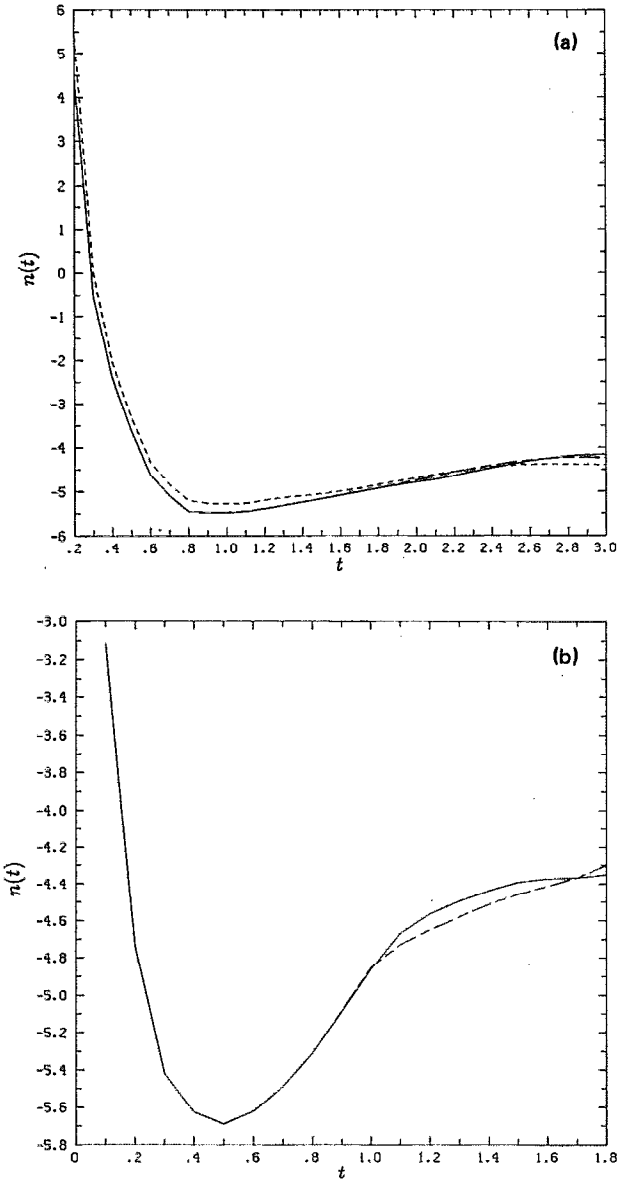

FIG. 7. Prefactor $n(t)$ versus time obtained by fitting the energy spectrum for the Taylor–Green vortex (a) and for the general periodic flow (b) in the same conditions as Figs. 2 and 5, respectively.

reported in Ref. 13. A consequence of this spectral behavior is that, as already noticed, the enstrophy is not dominated by the smallest scales.

IV. FORMATION OF VORTEX LAYERS

The decay in time of the logarithmic decrement measured on the energy spectrum has a counterpart in physical space where it is associated with the generation of small-scale structures. In order to characterize this process, we choose to visualize the high vorticity regions of the flow. For both the Taylor–Green vortex and the general periodic flow, we observe the formation of pancakelike structures whose thickness decays in time.

In the case of the Taylor–Green vortex, the pancake is formed near the center of the $y=0$ face which is a mirror symmetry plane of the flow. Figure 8 displays the vorticity in this plane at times $t=3$, 3.25, 3.50, and 4. Shorter times ($t=0$ and 2) were given in Fig. 1 of Ref. 10. We clearly observe the formation of a vorticity layer which shrinks in time without significant distortion. This process is observed even when the layer becomes so thin that its inner structure is not longer accurately resolved. A model based on the special geometry of the Taylor–Green vortex and, in particular, the convergence of the fluid at $z=\pi/2$, was presented in Ref. 10 (Appendix 4) and predicts an exponential decay for the width of the analyticity strip of the solution.

The formation of vorticity layers is in fact generic for a three-dimensional ideal flow. In Fig. 9, high vorticity regions are represented for the general periodic flow at times $t=0.05$, 1.10, 1.65, and 2.95. The visualizations were done on a Silicon Graphic machine, using the (three-dimensional) interactive Vector Field Flight Simulator software developed at CERFACS in Toulouse. We see that initially isotropic blobs of vorticity contract in one direction, while in the two others, the dimensions remain finite.

In order to reproduce the dynamics of an isolated pancake structure in a more general context, we construct a simple self-similar model by looking for a velocity field of the form

$$v_i=M_i(t)w_i(\xi_1,\xi_2,\xi_3) \tag{8a}$$

and a pressure

$$p=N(t)P(\xi_1,\xi_2,\xi_3), \tag{8b}$$

where

$$\xi_i=x_i/l_i(t). \tag{9}$$

The incompressibility condition leads to

$$\sum_j \frac{M_j}{l_j}\frac{\partial w_j}{\partial \xi_j}=0, \tag{10}$$

while the momentum equation gives

$$\frac{\dot{M}_i}{M_i}w_i+\sum_j\left(-\frac{\dot{l}_j}{l_j}\xi_j\frac{\partial}{\partial\xi_j}+\frac{M_j}{l_j}w_j\frac{\partial}{\partial\xi_j}\right)w_i=-\frac{N}{l_iM_i}\frac{\partial P}{\partial\xi_i}, \tag{11}$$

where overdots denote time derivatives.

Assuming that the pancake structure shrinks in the ξ_3 direction, while the characteristic scales in the transverse directions remain of order unity, a solution of Eqs. (10) and (11) consistent with this evolution corresponds to the scaling factors

$$M_1=M_2=1,\quad l_1=l_2=1;$$
$$M_3=l_3=e^{-t/T},\quad N=1. \tag{12}$$

The profile of the solution is given by the system

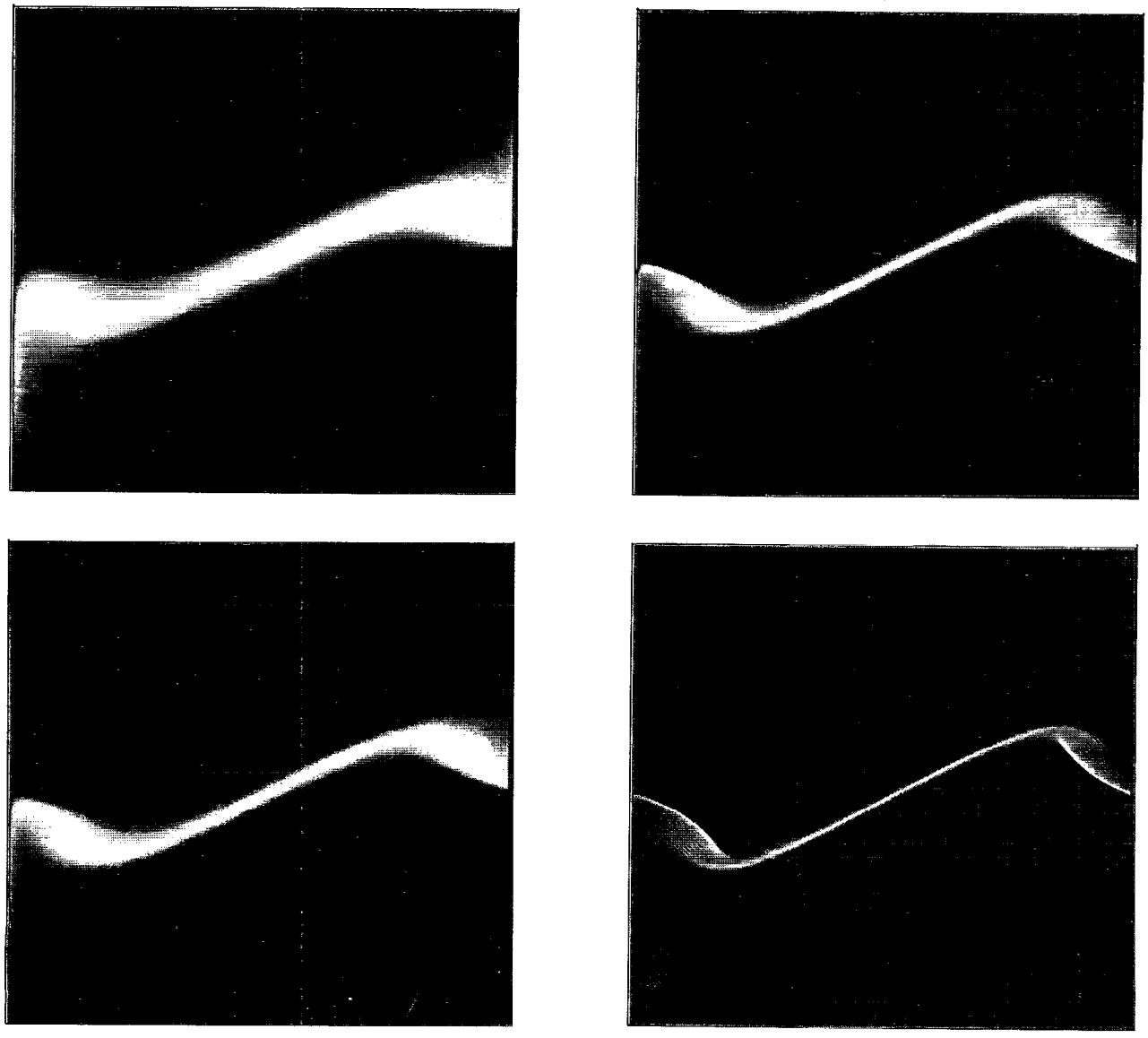

FIG. 8. Visualizations in physical space of high vorticity regions for the Taylor–Green vortex at $t=3$, 3.25, 3.50, and 4. Note that the thickness of the pancake decays in time.

$$\nabla_\perp \cdot w_\perp + \frac{\partial w_3}{\partial \xi_3} = 0,$$

$$\frac{\xi_3}{T}\frac{\partial w_\perp}{\partial \xi_3} + \left(w_\perp \cdot \nabla_\perp + w_3 \frac{\partial}{\partial \xi_3} \right) w_\perp = -\nabla_\perp P, \tag{13}$$

$$\frac{\partial P}{\partial \xi_3} = 0,$$

where $\perp$ denotes the projection in the plane perpendicular to the ξ_3 direction. We notice that, as is usually the case for a boundary layer, the pressure does not change significantly when crossing the pancake. Note that although space dimension does not explicitly enter in the above scaling, no nonzero solutions of Eq. (13) can be considered in the context of two-dimensional flows since the vorticity

$$\omega = \text{curl } \mathbf{v} = \begin{pmatrix} -e^{t/T}\dfrac{\partial w_2}{\partial \xi_3} \\ e^{t/T}\dfrac{\partial w_1}{\partial \xi_3} \\ 0 \end{pmatrix} + O(1) \tag{14}$$

grows exponentially in time, while it is conserved in two dimensions.

It is interesting to consider the strain matrix

$$\mathbf{S} = \frac{1}{2}(\nabla \mathbf{v} + \nabla \mathbf{v}^{\text{tr}})$$

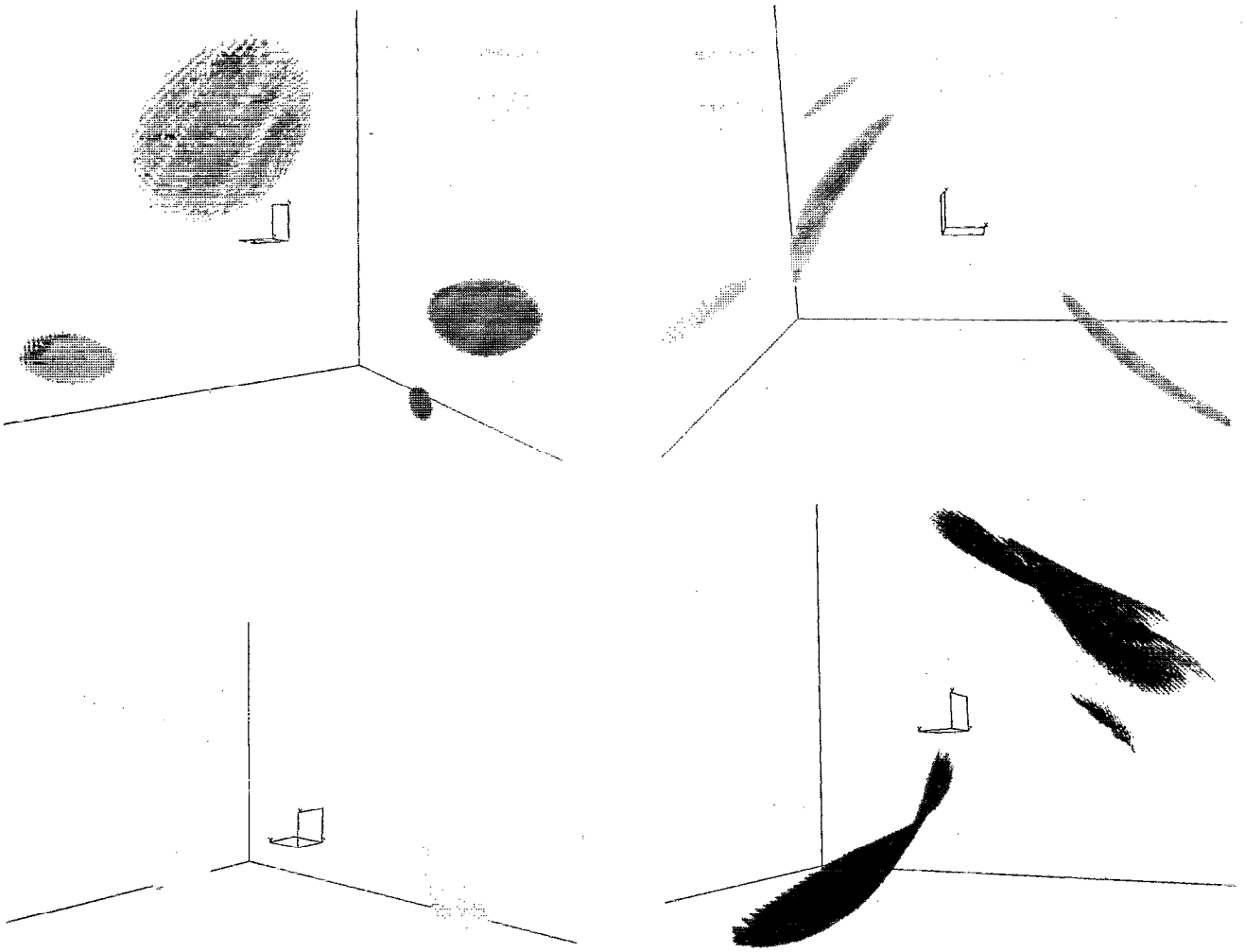

FIG. 9. High vorticity regions for the random flow at times $t=0.05$, 1.10, 1.65, and 2.95.

$$=\frac{1}{2}\begin{pmatrix} 0 & 0 & e^{t/T}\dfrac{\partial w_1}{\partial \xi_3} \\ 0 & 0 & e^{t/T}\dfrac{\partial w_2}{\partial \xi_3} \\ e^{t/T}\dfrac{\partial w_1}{\partial \xi_3} & e^{t/T}\dfrac{\partial w_2}{\partial \xi_3} & 0 \end{pmatrix}+O(1). \tag{15}$$

It is easily checked that the eigenvalues of $\mathbf{S}$ read

$$\lambda_1=\frac{1}{2}e^{t/T}\sqrt{\left(\frac{\partial w_1}{\partial \xi_3}\right)^2+\left(\frac{\partial w_2}{\partial \xi_3}\right)^2}+O(1),$$

$$\lambda_2=O(1), \tag{16}$$

$$\lambda_3=-\lambda_1.$$

The associated eigenvectors are

$$\mathbf{V}_1=e^{t/T}\left[\frac{\partial w_1}{\partial \xi_3},\frac{\partial w_2}{\partial \xi_3},\sqrt{\left(\frac{\partial w_1}{\partial \xi_3}\right)^2+\left(\frac{\partial w_2}{\partial \xi_3}\right)^2}\right]+O(1),$$

$$\mathbf{V}_2=e^{t/T}\left(\frac{\partial w_2}{\partial \xi_3},-\frac{\partial w_1}{\partial \xi_3},0\right)+O(1), \tag{17}$$

$$\mathbf{V}_3=e^{t/T}\left[\frac{\partial w_1}{\partial \xi_3},\frac{\partial w_2}{\partial \xi_3},-\sqrt{\left(\frac{\partial w_1}{\partial \xi_3}\right)^2+\left(\frac{\partial w_2}{\partial \xi_3}\right)^2}\right]+O(1).$$

Our model thus predicts that the vorticity tends to be aligned with the strain eigenvector associated to the (finite) intermediate eigenvalue. Furthermore, the two other eigenvectors make an angle of $\pi/4$ with the ξ_3 axis.

The alignment of vorticity with the intermediate strain eigenvector was conjectured by Vieillefosse[18] on the basis of a simplified analysis where the pressure is supposed to act in a completely isotropic way. As discussed in Refs. 19 and 20, this assumption, which leads to a finite time blowup of the vorticity, is likely to become inconsistent as the singularity is approached and to change the dynamical picture drastically. Vieillefosse's prediction concerning the

vorticity direction, is however, preserved in the revised models presented in Ref. 19 where the (nonlocal) anisotropic pressure effects are heuristically modeled in terms of prescribed random coefficients. The influence of these nonlocal effects on vortex stretching and alignment is in fact not fully understood. A formalism that clearly identifies the various competing factors was recently proposed in Ref. 20.

Coming back to our self-similar model, an explicit solution of Eq. (13) that explains some of the features seen in the visualizations of our numerical simulations (see below) is obtained in the form

$$w_1=f(\xi_3),$$
$$w_2=\xi_2/T, \tag{18}$$
$$w_3=-\xi_3/T,$$

or equivalently, when coming back to the primitive variables

$$v_1=f(ze^{t/T}),$$
$$v_2=y/T, \tag{19}$$
$$v_3=-z/T.$$

Note that this velocity is in fact an exact solution of the Euler equation. It corresponds to the superposition of a shear flow [associated to a vortex layer in the (x,y) plane] and a uniform strain field in the (z,y) plane.

Computing strain and vorticity for this flow, one obtains (setting $T=1$)

$$\mathbf{S}=\begin{pmatrix}0 & 0 & \alpha\\ 0 & 1 & 0\\ \alpha & 0 & -1\end{pmatrix} \tag{20}$$

and

$$\omega=\begin{pmatrix}0\\ 2\alpha\\ 0\end{pmatrix}, \tag{21}$$

with

$$\alpha=e^t f'(ze^t). \tag{22}$$

The eigenvalues of $\mathbf{S}$ are

$$\lambda_1=-\tfrac{1}{2}+\sqrt{\alpha^2+\tfrac{1}{4}},$$
$$\lambda_2=1, \tag{23}$$
$$\lambda_3=-\tfrac{1}{2}-\sqrt{\alpha^2+\tfrac{1}{4}},$$

with the associated eigenvectors

$$\mathbf{V}_1=(\alpha,0,-\tfrac{1}{2}+\sqrt{\alpha^2+\tfrac{1}{4}}),$$
$$\mathbf{V}_2=(0,1,0), \tag{24}$$
$$\mathbf{V}_3=(\alpha,0,-\tfrac{1}{2}-\sqrt{\alpha^2+\tfrac{1}{4}}).$$

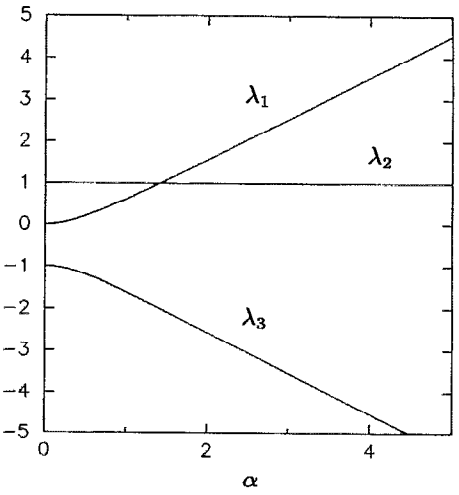

FIG. 10. Variation of the strain eigenvalues with the parameter α, defined in (22).

Figure 10 displays the variations of the eigenvalues as a function of α. We notice that λ_1 and λ_2 cross each other for $\alpha=\sqrt{2}$. The self-similar regime discussed at the beginning of this section corresponds to α large compared to the crossing value. The model (19) illustrates the evolution toward this asymptotic regime. We note that the strain eigenvector $\mathbf{V}_2$ remains aligned with the vorticity. In contrast $\mathbf{V}_1$ and $\mathbf{V}_3$ rotate in time in the (x,z) plane. While for small α (short times) the contracting direction $\mathbf{V}_3$ is perpendicular to the vorticity layer [which is parallel to the (x,y) plane], for large α (long times), it becomes inclined at 45° relative to the layer. Already when the eigenvalues cross each other, the angle is close to 55°. The same inclination of 45° is displayed by the dominantly expanding direction $\mathbf{V}_1$, in the long time regime.

In order to validate the dynamics as exemplified by the above model, we have simultaneously visualized the vorticity and the strain eigenvectors in regions of strong vorticity. These visualizations, done for the general periodic flow, support both the alignment of vorticity with the intermediate eigenvector and the rotation in time of the two other eigenvectors toward a direction making an angle of $\pi/4$ with the vortex layer. The interactive change of viewpoint provided by VFFS software enabled us to obtain a rather clear representation of the direction of the vectors. In contrast, a fixed picture is ambiguous in this respect and is thus not shown.

To get a quantitative insight, we have computed the histograms of the cosines of the angles between the vorticity and the three eigenvectors in the regions where the former exceeds 50% of its maximum. The results displayed in Fig. 11 confirm the alignment of the vorticity with the intermediate eigenvector.

V. COLLAPSE OF VORTEX LAYERS AND GENERATION OF VORTEX TUBES

The stability of a stretched vortex layer of the type described by (19) when slowly modulated in the x direc-

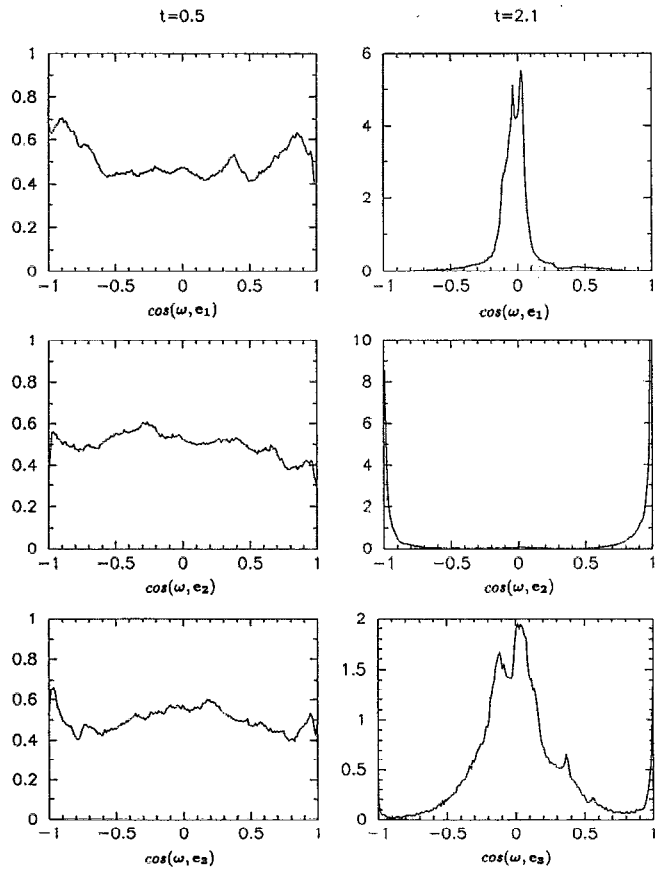

FIG. 11. Histograms of the cosines of the angles between the vorticity ω and the three strain matrix eigenvectors $\mathbf{e}_1$, $\mathbf{e}_2$, and $\mathbf{e}_3$, associated to the eigenvalues in ascending order, for the random periodic flow at times t=0.5, and 2.1.

tion was studied in the context of free shear layers to model the formation of streamwise vortices.[21,22] This analysis sheds light on the dynamics of the vorticity pancakes described in Sec. IV, beyond the time at which the integration has to be stopped due to loss of accuracy. In contrast with vorticity pancakes for which the vorticity is always directed in the expansion direction of the external strain [see Eq. (21)], in free shear layers the initial vorticity is mostly perpendicular to both the contraction and the expansion direction of the strain field resulting from the Kelvin–Helmholtz roll-up of the free shear layer. After a while, however, this vorticity aligns with the expansion direction of the strain. The subsequent dynamics of free shear layers, as modeled in Refs. 21 and 22, identifies with the stability problem of our vorticity pancakes. Both asymptotic analysis[21] and numerical simulations[22] indicate that the vorticity focuses in a finite time into streamwise filaments. Reinterpreted in the context of our problem, this corresponds to a catastrophic collapse (in the x direction) of the vorticity pancake. This mechanism proceeds until the typical width and thickness become comparable, forming a vortex tube.

The external strain will continue to shrink exponentially the resulting vortex tubes.[23] However, self-interactions and/or interactions among vortex filaments may possibly lead to a more singular behavior.[24–26] Still, the conclusions of numerical simulations of interacting vortex tubes are controversial about the existence of a finite time singularity.[7,12,13]

In the context of Navier–Stokes flows at large Reynolds numbers, the shrinking of a vorticity pancake is stopped by viscosity. The resulting vortex layer (with a small but finite thickness) collapses like in an ideal fluid. This process is interrupted when the width of the structure becomes comparable to its thickness. A vortex filament aligned with the intermediate strain eigenvector have then been formed, similar to those observed in numerical simulations of fully developed turbulence.[15,16,27–30] Furthermore, the time for filament formation has a finite limit as viscosity tends to zero. This is a consequence of the catastrophic collapse of an infinitely thin vortex sheet.[21] This quasisingular behavior provides an interpretation to the abrupt formation of vorticity filaments observed in a recent experiment.[31]

VI. CONCLUSION

We have simulated numerically the short-time dynamics of space-periodic three-dimensional ideal flows whose energy is initially concentrated in the largest scales. Both highly symmetric and randomly chosen initial conditions were considered. Since the nonlinearities lead to the development of arbitrarily small scales, the computation was limited to the time during which all the scales of motion were accurately resolved. After an early transient, we observed an exponential decay in time for the logarithmic decrement of the energy spectrum, or equivalently for the width of the analyticity strip of the velocity field. A simple model assuming a self-similar dynamics was also presented and satisfactorily compared with numerical observations.

We suggest that, like in free shear layers, the subsequent dynamics consists in focusing instabilities which concentrate the vorticity leading to abrupt generation of isolated vortex filaments. The possible existence of a finite time singularity for the Euler equation may strongly depend on the details of the interactions between these structures. In this picture, the elementary processes leading to the formation of small-scale structures in turbulent flows are of a purely inviscid origin. Viscosity prescribes minimal scales and permits reconnection.

ACKNOWLEDGMENTS

We are grateful to R. Krasny for pointing out Ref. 21 to our attention. The calculations were done on the Cray-2 of the Centre de Calcul Vectoriel Pour la Recherche (Palaiseau, France). The main routine used in all our calculations is the fast Fourier transform of the Cray-2 library, which is a *C.* Temperton FFT adapted for this machine by Cray Research.

One of us (MEB) acknowledges the support of Grant No. 90-173 from the Direction des Recherches Etudes et Techniques.

[1] C. Bardos and U. Frisch, "Régularité d'un fluide parfait de données

initiales Hölderiennes," C. R. Acad. Sci. Ser. A **281**, 775 (1975); "Finite-time regularity for bounded and unbounded ideal incompressible fluids using Hölder estimates," in *Turbulence and Navier–Stokes Equations*, Lecture Notes in Mathematics, edited by R. Temam (Springer-Verlag, Berlin, 1976), Vol. 565, p. 1.
[2]C. Bardos and S. Benachour, "Domain d'analyticité des solutions de l'équation d'Euler dans un ouvert de R^n," Ann. Sci. Norm. Super. Pisa, Ser. IV **4**, 647 (1977).
[3]T. Kato, "Nonstationary flows of viscous and ideal fluids in R^3," J. Funct. Anal. **9**, 296 (1972).
[4]J. T. Beale, T. Kato, and A. Majda, "Remarks on the breakdown of smooth solutions for 3-D Euler equations," Commun. Math. Phys. **94**, 61 (1984); G. Ponce, "Remarks on a paper by J. T. Beale, T. Kato, and A. Majda," Commun. Math. Phys. **98**, 349 (1985).
[5]H. A. Rose and P. L. Sulem, "Fully developed turbulence and statistical mechanics," J. Phys. (Paris) **39**, 441 (1978).
[6]S. A. Orszag, "Statistical theory of turbulence," in *Fluids Dynamics; 1973—Les Houches Summer School of Physics*, edited by R. Balian and J. L. Peube (Gordon and Breach, New York, 1977), p. 235.
[7]R. M. Kerr and F. Hussain, "Simulation of vortex reconnection," Physica D **37**, 474 (1989).
[8]R. H. Morf, S. A. Orszag, and U. Frisch, "Spontaneous singularity in three-dimensional inviscid incompressible flow," Phys. Rev. Lett. **44**, 572 (1980).
[9]G. I. Taylor and A. E. Green, Mechanism of the production of small eddies from large one," Proc. R. Soc. London Ser. A **158**, 499 (1937).
[10]M. Brachet, D. Meiron, S. A. Orszag, B. Nickel, R. Morf, and U. Frisch, "Small-scale structure of the Taylor–Green vortex," J. Fluid Mech. **130**, 411 (1983).
[11]A. Pumir and E. D. Siggia, "Collapsing solutions of the 3-D Euler equation," Phys. Fluids A **2**, 220 (1990).
[12]A. Pumir and E. D. Siggia, "Development of singular solutions of the axisymmetric Euler equation," Phys. Fluids A **4**, 1472 (1992).
[13]R. M. Kerr, "Evidence for a singularity of the three-dimensional incompressible Euler equation," preprint (unpublished).
[14]C. Sulem, P. L. Sulem, and H. Frisch, "Tracing complex singularities with spectral methods," J. Comput. Phys. **50**, 138 (1983).
[15]M. E. Brachet, "Direct simulation of three-dimensional turbulence in the Taylor–Green vortex," Fluid Dyn. Res. **8**, 1 (1991).
[16]A. Vincent and M. Meneguzzi, "The spatial structure and statistical properties of homogeneous turbulence," J. Fluid Mech. **225**, 1 (1991).
[17]S. A. Orszag and G. S. Patterson, "Numerical simulation of the three-dimensional homogeneous turbulence," Phys. Rev. Lett. **28**, 76 (1972).
[18]P. Vieillefosse, "Local interaction between vorticity and shear in a perfect incompressible fluid," J. Phys. (Paris) **43**, 837 (1982).
[19]Z. S. She, E. Jackson, and S. A. Orszag, "Structure and dynamics of homogeneous turbulence: Models and simulations," Proc. R. Soc. London Ser. A **434**, 101 (1991).
[20]E. Dresselhaus and M. Tabor, "The kinematics of stretching and alignment of material elements in general flow fields," J. Fluid Mech. **236**, 415 (1992).
[21]J. C. Neu, "The dynamics of stretched vortices," J. Fluid Mech. **143**, 253 (1984).
[22]S. J. Lin and G. M. Corcos, "The mixing layer: Deterministic models of a turbulent flow. Part 3. The effect of plane strain on the dynamics of streamwise vortices," J. Fluid Mech. **141**, 139 (1984).
[23]J. C. Neu, "The dynamics of a columnar vortex in an imposed strain," Phys. Fluids **27**, 2397 (1984).
[24]A. J. Chorin, "The evolution of a turbulent vortex," Commun. Math. Phys. **83**, 517 (1982).
[25]E. D. Siggia, "Collapse and amplification of a vortex filament," Phys. Fluids **28**, 794 (1985); A. Pumir and E. D. Siggia, "Vortex dynamics and the existence of solutions to the Navier–Stokes equations," Phys. Fluids **30**, 1606 (1987).
[26]A. Fukuyu and T. Arai, "Singularity formation in three-dimensional inviscid flow," Fluid Dyn. Res. **7**, 229 (1991).
[27]E. D. Siggia, Numerical study of small-scale intermittency in three-dimensional turbulence" J. Fluid Mech. **107**, 375 (1981).
[28]R. M. Kerr, "Higher-order derivative correlations and the alignment of small-scale structures in isotropic numerical turbulence," J. Fluid Mech. **153**, 31 (1985).
[29]W. T. Ashurst, A. R. Kerstein, R. M. Kerr, and C. H. Gibson, "Alignment of vorticity and scalar gradient with strain rate in simulated Navier–Stokes turbulence," Phys. Fluids **30**, 2343 (1987).
[30]Z. S. She, E. Jackson, and S. A. Orszag, "Intermittent vortex structures in homogeneous isotropic turbulence," Nature **344**, 226 (1990).
[31]S. Douady, Y. Couder, and M. E. Brachet, "Direct observation of the intermittency of intense vorticity filaments in turbulence," Phys. Rev. Lett. **67**, 982 (1991).